NANOMEETING-2019

Второй день конференции

Poster session

В завершение второго дня конференции прошла секция ***Poster session***. Выставленные доклады привлекли большое внимание участников. Обсуждения проходили активно у каждого стенда, ведь это прекрасная возможность побеседовать с авторами, найти ответы на свои вопросы и, наконец, поближе познакомиться с участниками конференции.

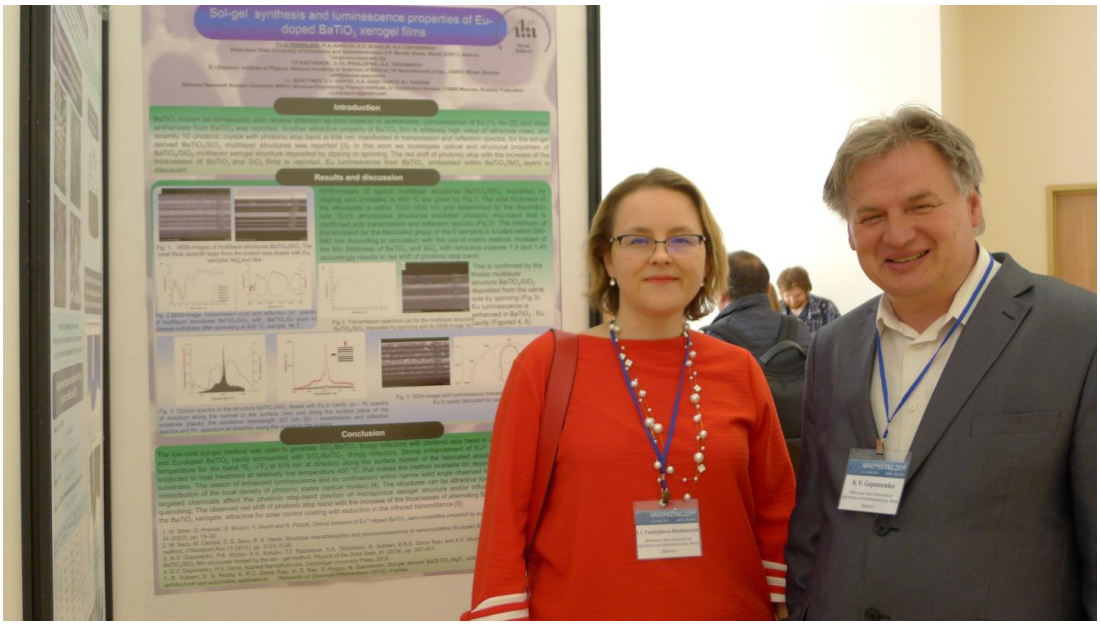

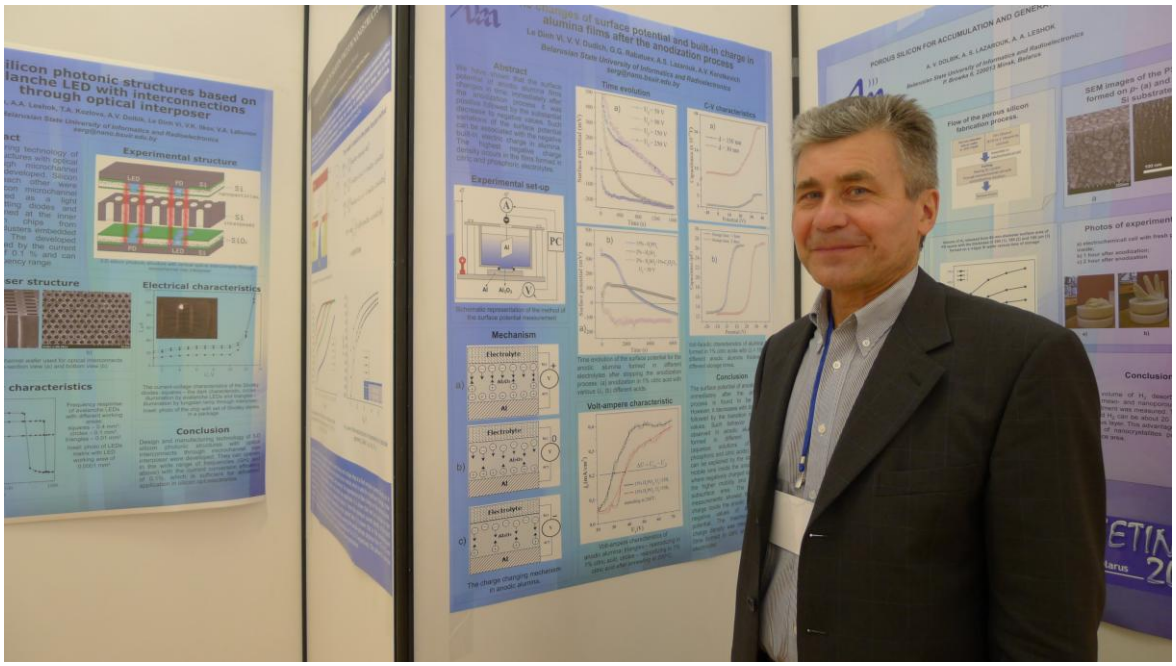
Experimental structure
Electrical characteristics
Conclusion
Experimental set-up
Mechanism
Volt-ampere characteristic

Практически все доклады красочно и информативно оформлены (к сожалению фото не может передать впечатление точно), и участники конференции внимательно изучают содержание докладов.

Вот некоторые из докладов:

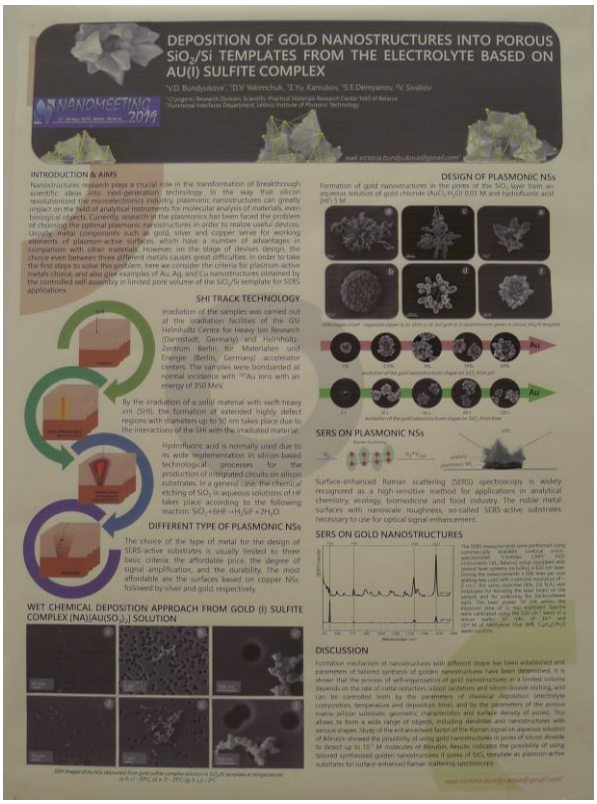

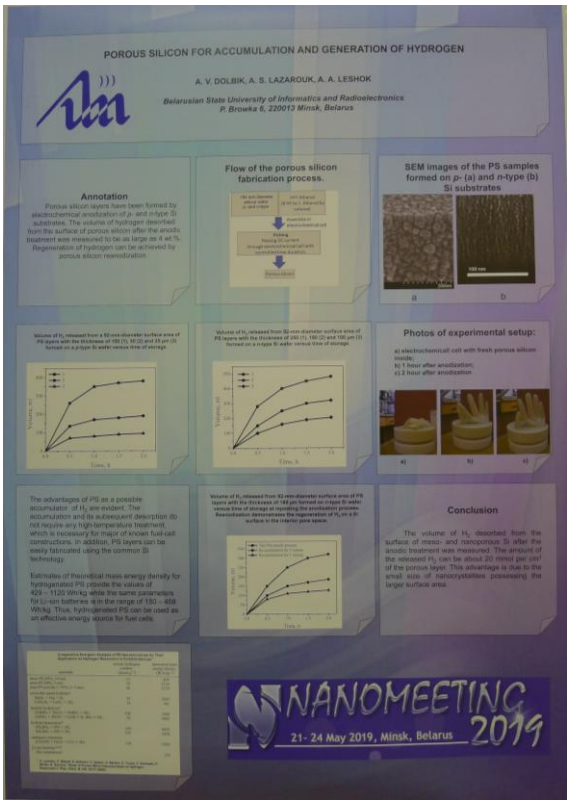

EXTREME HEATING OF ALUMINA BARRIER LAYER DURING HIGH ELECTRIC FIELD ANODIZATION OF ALUMINUM

O. Kupreeva[1], G. Rabatuev[2], V. Dudich[1], T. Orehovskaia[1], S. Lazarouk[1,2]
[1]Belarusian State University of Informatics and Radioelectronics, Minsk, Belarus
[2]National Research Nuclear University MEPhI, Moscow, Russia
e-mail: Olga_Kupreeva@bsuir.by

Motivation of Investigation

The temperature of alumina barrier layer during a high electric field anodization of aluminum (the current density more than 50 mA/cm²) has been studied by analyzing the aluminum film resistance. In the case of Joule heat power density to be larger than 20 W/cm², the temperature inside the barrier layer can exceed 660 °C, which leads to the local melting of aluminum. Scanning electron microscopy has shown the location of molten aluminum droplets and their movement during the anodization process.

SEM images of experimental structures showing local melting of aluminum during the high field porous aluminum anodization

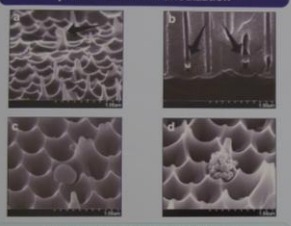

a) aluminum drop emerging on aluminum peak,
b) the movement of aluminum droplets through the alumina pores,
c,d) top view of aluminum droplets solidified in the pore mouths.

The scheme of the experimental cell

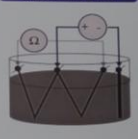

Distribution of electric field strength and Joule heating specific power inside the porous alumina barrier layer

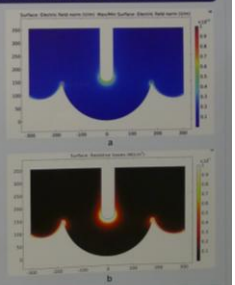

a) distribution of electric field strength,
b) distribution of Joule heating specific power.

The experiment based calculations of heat transfer coefficient (HTC)

Heat transfer coefficient:

$$h = Nu \cdot Km / L$$

Nusselt number:

$$Nu = 0.68 + 0.67 \cdot (Gr \cdot Pr)^{1/4} \cdot \left[1 + (0.492/Pr)^{9/16}\right]^{-4/9}$$

Grashof number:

$$Gr = g \cdot L^3 \cdot \beta \cdot \Delta T / \nu^2$$

Temperature difference between electrolyte and heated surface:

$$\Delta T = T_e - T_0 = P_s / h$$

Electrolyte temperature	Electrolyte density	Kinematic viscosity	Specific heat	Thermal conductivity	Thermal diffusivity	TCE	Prandtl number
T_0, °C	ρ, kg/m³	ν, 10^{-6} m²/s	c_p, J/(kg·K)	K_m, W/(m·K)	a, 10^{-8} m²/s	β, 10^{-4} K⁻¹	Pr
-10	1 137.03	40.55	2 249.30	0.24	92.80	0.62	1 027.24
0	1 130.00	41.50	2 254.00	0.24	93.80	0.62	958.77
10	1 122.97	40.40	2 338.70	0.25	93.70	0.63	431.81
20	1 115.94	39.60	2 383.40	0.25	93.90	0.63	260.25
40	1 101.88	11.50	2 472.80	0.26	93.90	0.64	132.55
60	1 087.82	4.58	2 562.20	0.26	93.30	0.65	50.29
80	1 073.76	2.15	2 651.60	0.26	92.20	0.65	23.35
100	1 060.70	0.93	2 741.00	0.26	90.80	0.66	10.28

L – the characteristic size of the heat exchange surface, defined as the ratio of the area to the perimeter

Conclusion

We have established that the temperature of the anodic alumina barrier layer during the high field (hard) anodization of aluminum can exceed 100 °C. When the electric power density is higher than 20 W/cm², the temperature inside this barrier layer can reach the aluminum melting point. That was confirmed by SEM observation of the structures formed at these regimes

FIELD EMISSION IN SILICON VACUUM NANOSTRUCTURE

A. G. Trafimenko, D. A. Podryabinkin, A. L. Danilyuk
Belarusian State University of Informatics and Radioelectronics, P. Browki Str. 6, 220013 Minsk, Belarus.

Abstract

The results of modeling of transmission coefficient and field emission current in a silicon vacuum nanostructure with a pyramidal cathode by means of phase function method are presented. Dependencies of these parameters on applied bias, size of the cathode and distance between anode and cathode are established. It is shown that in such nanostructure the field emission current density of 1-10 A/cm2 can be achieved by varying the distance between anode and cathode in the range of 15-25 nm and the applied bias in the range of 1.2 to 2.3 V.

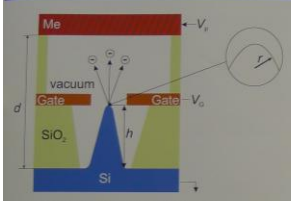

Cross-section of the vacuum nanostructure

The model is based on the phase function method

$$\frac{dB(z)}{dz} = -\frac{U(z)}{2ik}\left[\exp(ikz) + B(z)\exp(-ikz)\right]^2$$

$$\frac{d\alpha(z)}{dz} = \frac{U(z)}{2k}\left[-\sin(2kz) - 2b + (a^2 - b^2)\sin(2kz) - 2ab\cos(2kz)\right]$$

$$\frac{d\beta(z)}{dz} = \frac{U(z)}{2k}\left[\cos(2kz) + 2a + (a^2 - b^2)\cos(2kz) - 2ab\sin(2kz)\right]$$

$$T(k) = \exp\left[-\frac{1}{k}\int_0^l U(z)\left[b(z)\cos(2kz) - a(z)\sin(2kz)\right]dz\right]$$

$$J = q\int N(k)T(k)dk$$

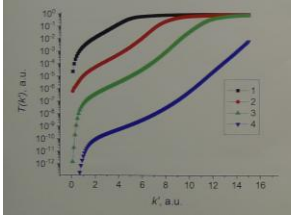

The dependence of the transmission coefficient on the wave number k' at various external bias V_p: 5 V (1), 3 V (2), 2.2 V (3), 1.5 V (4).

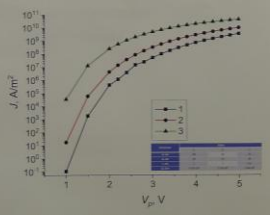

I-V curve of the nanostructures in dependence of cathode geometry. Table: 1-a, 2-b, 3-c.

Conclusion

We calculated the transmission coefficient, emission current density and voltage drop at a fixed emission current density in a silicon nanostructure with a pyramidal cathode using the phase function method, which is valid for a significant change in the potential energy at the de Broglie electron wavelength, are presented. The dependencies of their change on the external bias, the cathode size and the distance between anode and cathode are established. It is shown that with an increase in the amplification coefficient of the field strength at the cathode tip of about 2 times the maximum current density of the field emission increases by 1-2 orders of magnitude in dependence on the applied bias. It is shown that in the nanostructure presented the emission current density of 1 A/cm² can be produced by varying the anode-cathode distance from 15 to 25 nm at external bias of 1.2-2.0 V, and the current density 10 A/cm²– at external bias of 1.4-2.3 V, respectively. This allows to use this structure as a basis for creation of elements for vacuum nanoelectronics of future generations.

STABILITY OF 2D ALKALINE-EARTH METAL SILICIDES, GERMANIDES, AND STANNIDES

A. Yu. Alekseev, A. G. Chernykh, A. B. Filonov, D. B. Migas
Belarusian State University of Informatics and Radioelectronics
Minsk, Belarus
E-mail for contact: lucky.alexey94@gmail.com

PURPOSE AND MOTIVATION

- Theoretical prediction of 2D alkaline-earth metal silicides, germanides and stannides.
- 2D alkaline-earth metal silicides, germanides, and stannides are semiconductors that can be compatible with the common silicon technology, can have promising optical properties and consist of environmentally friendly and abundant in the Earth crust atoms.

COMPUTATIONAL METHODS AND DETAILS

- Density functional theory (DFT).
- Perdew–Burke–Ernzerhof (PBE) approximation.
- Cutoff energy 360 eV.
- Vacuum thickness 12 Å.
- 3×3×1 supercell and Γ-centered 6×6×1 *k*-mesh for calculations of harmonic FCs of T-phase structures.
- 4×2×1 supercell and Γ-centered 3×4×1 *k*-mesh for calculations of harmonic FCs of Td-phase structures.
- Vienna *Ab-initio* Simulation Package (VASP).

STRUCTURE

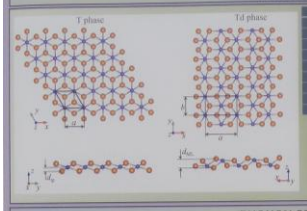

	a_0, Å	b_0, Å	d_{Ca-X}, Å
T-Ca_2Si	4.72	2.96	1.15
T-Sr_2Si	4.93	3.13	1.31
T-Ba_2Si	5.10	3.31	1.50
T-Ca_2Ge	4.75	2.98	1.16
T-Sr_2Ge	4.96	3.15	1.32
T-Ba_2Ge	5.12	3.32	1.51
T-Ca_2Sn	5.07	3.15	1.15
T-Sr_2Sn	5.28	3.32	1.31
T-Ba_2Sn	5.44	3.48	1.51

	T-Mg_2X	Td-Mg_2X	Td-Ca_2X
$E_{f,coh}$, eV / f. u.	0.02	0.43	0.11
a_0, Å	7.28	7.31	7.40
b_0, Å	4.34	4.37	4.66
d_{Mg-X}, Å	2.65–2.68	2.68–2.70	2.86–2.91
d_{X-X}, Å	4.34–4.43	4.37–4.47	4.66–4.88
d_{Mg-Mg}, Å	2.03	2.07	2.26

PHONON SPECTRA

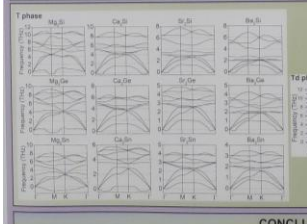

CONCLUSION

- The dynamical stability of 2D Td-phase Mg_2X and 2D T-phase Ca_2X, Sr_2X and Ba_2X is justified.
- The calculated imaginary frequencies in the phonon spectra of 2D Me2X in the vicinity of the Γ point can stem from the computational numerical inaccuracy because of the limited supercell size and the used harmonic approximation.

NON-POROUS NITROGEN AND RUTHENIUM CO-DOPED TITANIA FILMS FOR PHOTOCATALYSIS

O. Linnik[1,*], L. Khoroshko[2]
[1]Chuiko Institute of Surface Chemistry NAS of Ukraine, 17 General Naumov Str., 17, 03164 Kyiv, Ukraine
[2]Belarusian State University of Informatics and Radioelectronics P. Browka str., 6, 220013 Minsk, Belarus
*Corresponding author – oklinnik@yahoo.co.uk

Motivation

Contamination of aqueous media and soil by various organic and inorganic compounds requires the fabrication of new semiconductive materials sensitive to solar light. Titania is the most used photocatalyst due to its unique properties such as chemical stability, non-toxicity and high photocatalytic activity. However, it only absorbs in the UV part of the solar spectrum. An increase of the photocatalytic activity toward visible light can be achieved by titania modification with nonmetals, metal ions or even noble metal nanoparticles.

Photocatalytic behavior

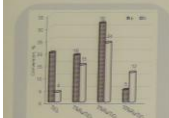

Photocatalytic activity of nitrogen free TiO_2 and Ru/TiO_2 films after irradiation by UV (a) and visible (b) light for 90 min

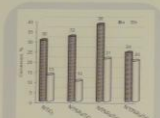

Photocatalytic activity of nitrogen doped TiO_2 and Ru/TiO_2 films after irradiation by UV (a) and visible (b) light for 90 min

Photocatalytic activity of the films under UV and visible light irradiation has been estimated in the processes of tetracycline hydrochloride (TC) degradation in 40 ml of its 2×10- 5 mol/L aqueous solution. The change in TC concentration was monitored with a Lambda 35 UV-vis spectrophotometer (PerkinElmer). The conversion percentage was calculated from the change in the absorption intensity at λ=357 nm. Prior to photocatalytic reactions, the adsorption equilibrium of film-liquid system was reached by stirring in the dark. A 1000 W mercury lamp was used for irradiation. A cut-off filter with λ = 380 nm was inserted to cut off UV light. The reaction did not proceed in the dark and in the presence of a bare glass instead of the film.

Structural investigation

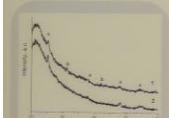

XRD patterns of N/5%Ru/TiO_2 (1) and 5%Ru/TiO_2 (2)

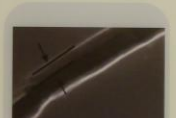

SEM image of N/5%Ru/TiO_2 film

XRD patterns of the films scratched off from the glass substrates have been performed on DRON-4.07 using Cu Kα irradiation (λ=1.5418 Å). They are presented at left. As it was shown, titania doping by urea led to crystallization of anatase and brookite compare to undoped titania films where only anatase was detected. For both N/5%Ru/TiO_2 and 5%Ru/TiO_2, the crystallization degree is lowered compare to TiO_2 and N/TiO_2, that can be caused by the presence of Ru ions. The XRD peaks at 25.3 (101), 37.9 (004), 48.1 (200), 54.1 (105) and 55.0 (211) deg are related to anatase formation (Fig. 3). The peaks at 31.2 (121) and 42.1 (231) deg observed only for N/5%Ru/TiO_2 can be a signed to brookite phase. Thus, nitrogen doping leads to the crystallization both anatase and brookite in 5%Ru/TiO_2.

Surface Properties

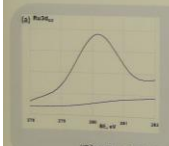

XPS spectra of $Ru3d_{5/2}$ (a) and 1Ns (b) for N/5%Ru/TiO_2

XPS lines of $Ti2p_{3/2}$ and $Ti2p_{1/2}$ with binding energy of 458.6 and 464.4 eV related to Ti(IV) surrounded by oxygen atoms, which are in the forms of O²⁻ ions and OH⁻ groups as evidenced by the XPS peaks at 529.8 and 531.4 eV, respectively, have been observed for 5%Ru/TiO_2 and N/5%Ru/TiO_2 films (not shown on left figure). The $Ru3d_{5/2}$ peak at 280.9 eV observed for both N/5%Ru/TiO_2 and 5%Ru/TiO_2 locates between the standard data of metallic Ru and Ru^{4+} in RuO_2. At the synthesis conditions used for the film preparation, the oxidation rather than reduction of Ru^{3+} ions occurred during sintering in air at 450 °C. The position of $Ru3d_{5/2}$ maximum (280.3 eV) is a signed to Ru^0 bonded through oxygen with less electronegative element. Thus, the incorporation of Ru ions in TiO_2 lattice takes place with formation of Ru–O–Ti bonds. Modification of the lattice of TiO_2 by nitrogen is proved by the appearance of N1s line within 394–403 eV for N/5%Ru/TiO_2, the two separated N1s peaks at 395.9 and 400 eV are fixed. The first one indicates on the presence of substitutional nitrogen atoms (N-Ti in titania lattice (N-Ti bonds), while the deconvoluted peaks of the second XPS line at 399.3, 400.1, 400.7 and 401.5 eV are related to the formation of N-O, N-H and/or N-C bonds.

Conclusion

Nitrogen and ruthenium co-doped titania films synthesized by sol-gel technique exhibit high photocatalytic activity under both UV and visible light. Incorporation of nitrogen and ruthenium ions in titania lattice is proven by XPS. Both doping agents affected structural properties of the films.

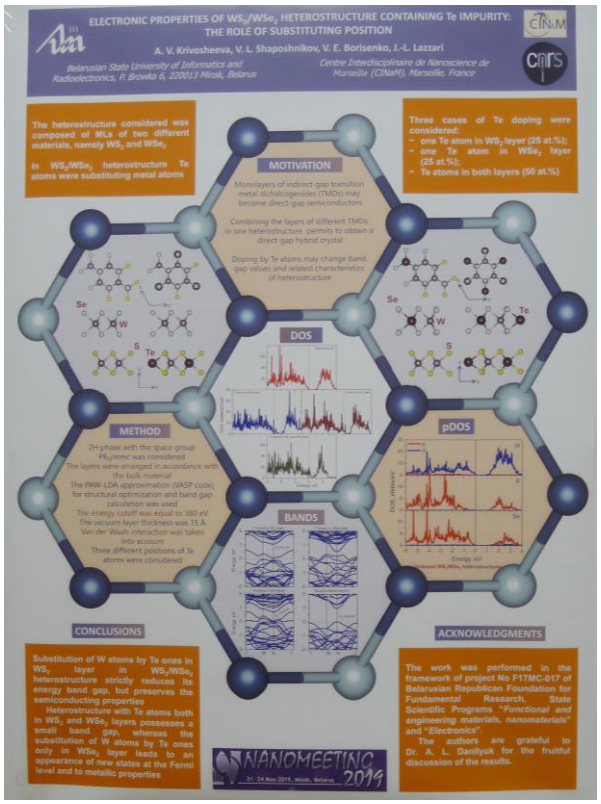
ELECTRONIC PROPERTIES OF WS_2/WSe_2 HETEROSTRUCTURE CONTAINING Te IMPURITY: THE ROLE OF SUBSTITUTING POSITION
A. V. Krivosheeva, V. L. Shaposhnikov, V. E. Borisenko, J.-L. Lazzari
Belarusian State University of Informatics and Radioelectronics, P. Browka 6, 220013 Minsk, Belarus
Centre Interdisciplinaire de Nanoscience de Marseille (CINaM), Marseille, France
The heterostructure considered was composed of MLs of two different materials, namely WS_2 and WSe_2.
In WS_2/WSe_2 heterostructure Te atoms were substituting metal atoms
MOTIVATION
Monolayers of indirect-gap transition metal dichalcogenides (TMDs) may become direct-gap semiconductors
Combining the layers of different TMDs in one heterostructure permits to obtain a direct-gap hybrid crystal
Doping by Te atoms may change band gap values and related characteristics of heterostructure
Three cases of Te doping were considered:
- one Te atom in WS_2 layer (25 at.%);
- one Te atom in WSe_2 layer (25 at.%);
- Te atoms in both layers (50 at.%)
DOS
pDOS
BANDS
METHOD
2H phase with the space group $P6_3/mmc$ was considered
The layers were arranged in accordance with the bulk material
The PAW-LDA approximation (VASP code) for structural optimization and band gap calculation was used
The energy cutoff was equal to 380 eV
The vacuum layer thickness was 15 Å
Van der Waals interaction was taken into account
Three different positions of Te atoms were considered
CONCLUSIONS
Substitution of W atoms by Te ones in WS_2 layer in WS_2/WSe_2 heterostructure strictly reduces its energy band gap, but preserves the semiconducting properties
Heterostructure with Te atoms both in WS_2 and WSe_2 layers possesses a small band gap, whereas the substitution of W atoms by Te ones only in WSe_2 layer leads to an appearance of new states at the Fermi level and to metallic properties
ACKNOWLEDGMENTS
The work was performed in the framework of project No F17MC-017 of Belarusian Republican Foundation for Fundamental Research, State Scientific Programs "Functional and engineering materials, nanomaterials" and "Electronics".
The authors are grateful to Dr. A. L. Danilyuk for the fruitful discussion of the results.
NANOMEETING 2019

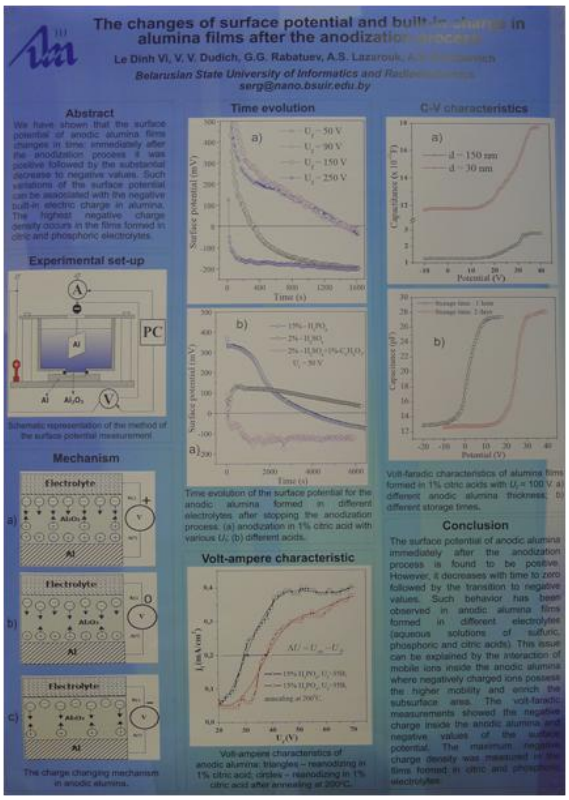
The changes of surface potential and built-in charge in alumina films after the anodization process
Le Dinh Vi, V. V. Dudich, G.G. Rabatuev, A.S. Lazarouk
Belarusian State University of Informatics and Radioelectronics
serg@nano.bsuir.edu.by
Abstract
Time evolution
C-V characteristics
Experimental set-up
Mechanism
Volt-ampere characteristic
Conclusion

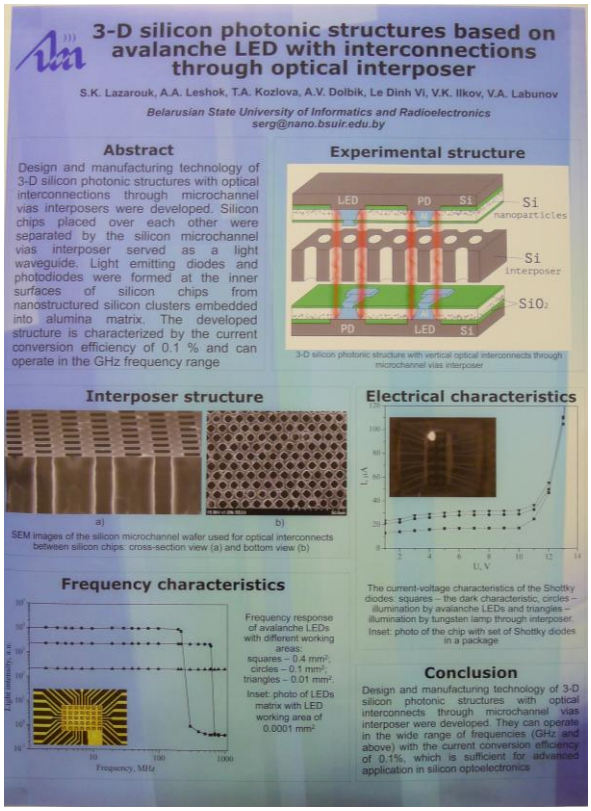
3-D silicon photonic structures based on avalanche LED with interconnections through optical interposer
S.K. Lazarouk, A.A. Leshok, T.A. Kozlova, A.V. Dolbik, Le Dinh Vi, V.K. Ilkov, V.A. Labunov
Belarusian State University of Informatics and Radioelectronics
serg@nano.bsuir.edu.by
Abstract
Experimental structure
Interposer structure
Electrical characteristics
Frequency characteristics
Conclusion

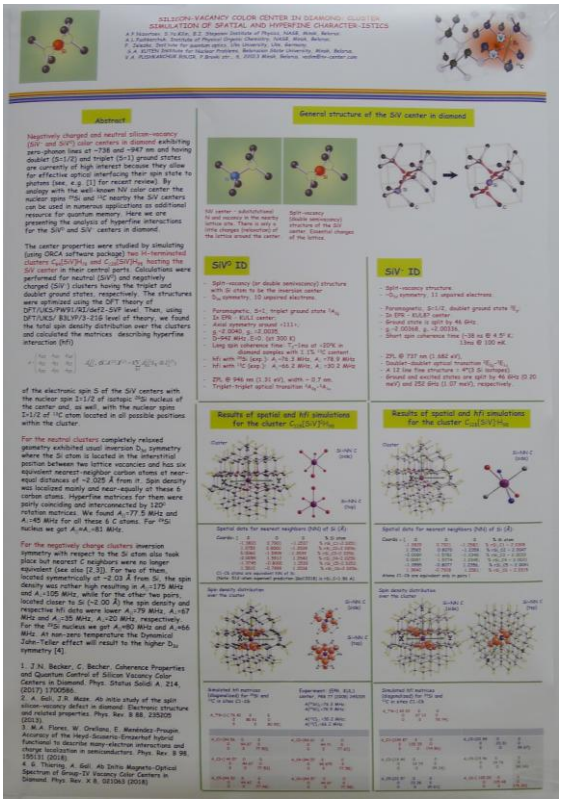
SILICON-VACANCY COLOR CENTER IN DIAMOND: CLUSTER SIMULATION OF SPATIAL AND HYPERFINE CHARACTERISTICS
Abstract
General structure of the SiV center in diamond
SiV⁰ ID
SiV⁻ ID
Results of spatial and hfi simulations for the cluster $C_{123}[SiV^0]H_{76}$
Results of spatial and hfi simulations for the cluster $C_{123}[SiV^-]H_{76}$